Nuclear Instruments and Methods in Physics Research B 287 (2012) 124–129

Contents lists available at SciVerse ScienceDirect

Nuclear Instruments and Methods in Physics Research B

journal homepage: www.elsevier.com/locate/nimb

Geant4 physics processes for microdosimetry simulation: Very low energy electromagnetic models for protons and heavy ions in silicon

A. Valentin [1,2], M. Raine [*,2], M. Gaillardin, P. Paillet

CEA, DAM, DIF, F-91297 Arpajon, France

ARTICLE INFO

Article history:
Received 3 April 2012
Received in revised form 25 May 2012
Available online 21 June 2012

Keywords:
Geant4-DNA
Energy-loss function
Inelastic cross-sections
Microdosimetry
Proton tracks
Ion tracks

ABSTRACT

The Geant4-DNA extension of the Geant4 Monte Carlo simulation toolkit aims at modeling early biological damages induced by ionizing radiation at the DNA scale, and it can now track particles down to very low energies in liquid water. New models, called "MuElec", have been implemented for microelectronic applications following the same initial theory, to track low energy electrons in silicon. This paper presents the extension of these MuElec models to incident protons and heavy ions in silicon. First, the theory of the model is presented. The resulting cross sections and stopping powers are compared with data from the literature. The model is then implemented in Geant4 and used to simulate proton tracks. Various physical quantities are extracted from the simulation, and compared with data from the literature and with results from simulation using other Geant4 models. It is shown that the generation of low-energy electrons results in more physically meaningful low-energy secondary electron tracks, which significantly modifies the proton and ion track core on the nanometer scale.

© 2012 Elsevier B.V. All rights reserved.

1. Introduction

The simulation of radiation effects in electronic systems is a critical concern in various domains, such as spacecraft missions or for instrumentation in nuclear power plants or medical equipments. With the decrease of size following the technological roadmap [1], accurate prediction of the sensitivity of electronic devices requires more and more detailed descriptions of ionization profiles. The Monte Carlo simulation toolkit Geant4 [2,3] is a suitable tool to address this issue and model the microscopic pattern of energy deposition related to an ionizing particle track structure, involving a detailed modeling of the trajectory of all secondary particles [4,5]. It has already been used successfully, in combination with TCAD simulations [6] or in SEE prediction tools [7,8], to study the sensitivity of advanced electronic devices, down to the 45 nm node. However, inherent limits in Geant4 ionization models prevent its use at smaller scales: the recommended production threshold energy of 250 eV for secondary electrons in the low energy electromagnetic package [9] limits the accuracy of the heavy ion track below 10 nm [6]. In order to study the effect of ionizing particles in future highly scaled integrated circuits by means of simulation, new ionization models are needed, lowering as much as possible this production threshold energy of secondary electrons.

Such models are already implemented in Geant4, but are restricted to water. These developments are part of the Geant4-DNA project, intended for biological applications [10,11]. To be used for microelectronic simulations, they need to be extended to other materials, silicon in particular. Various individual initiatives have been conducted over the years, but no open access version is available for the community. In particular, the work of Akkerman et al. aims at generating and tracking electrons down to an energy of 1.5 eV in silicon [12–15]. It relies on the same theoretical framework as the Geant4-DNA package for the calculation of ionization inelastic cross-sections. The goal of this paper is to use the approach described in [12–15] to calculate these cross-sections and to include them in the open-access frame of Geant4, using the already existing Geant4-DNA classes as a basis for implementation. This approach has already been used to describe electron energy losses in silicon [16,17]. This paper deals with the extension of the model to the generation of low energy electrons by incident protons and heavy ions. To avoid any confusion given the different domains of application, the new models are implemented separately from the Geant4-DNA extension, under the name "MuElec" (for microelectronics).

First, the theory used to calculate the inelastic cross-sections is presented. The main calculation steps are only briefly described, being similar for all incident particles and already extensively detailed in [16,17] for electrons. Various parameters are then calculated from these cross-sections and compared with data from the

* Corresponding author. Tel.: +33 169264058.
E-mail address: melanie.raine@cea.fr (M. Raine).
[1] Present address: LSPM-CNRS, Université Paris 13, 99 Avenue JB Clément, F-93430 Villetaneuse, France.
[2] Member of the Geant4 collaboration.

0168-583X/$ - see front matter © 2012 Elsevier B.V. All rights reserved.
http://dx.doi.org/10.1016/j.nimb.2012.06.007

literature to validate the implementation. Finally, resulting proton tracks in silicon simulated with MuElec models are presented. The differences between these tracks and those obtained using the low energy ionization models already available in Geant4 are particularly highlighted.

2. Theory

In Geant4-DNA for water and in the code by Akkerman et al. [12–14] for silicon, the inelastic interaction cross sections σ, are calculated using the complex dielectric function theory [18,19]. All calculations are based on the modeling of the Energy-Loss Function (ELF):

$$ELF(\hbar\omega,\vec{q}) = \mathrm{Im}\left[\frac{-1}{\varepsilon(\omega,\vec{q})}\right]$$

Where $\varepsilon(\omega,\vec{q})$ is the complex dielectric function, with $\hbar\omega$ and $\vec{q}$, respectively, the energy and momentum transfer from the incident particle to an electron of the target material. While the ELF is not easily measured, the Optical Energy-Loss Function (OELF), which is the particular case at $\vec{q}=\vec{0}$ can be deduced from experimental optical data [20,21]:

$$\mathrm{OELF} = \mathrm{ELF}(\hbar\omega,\overrightarrow{0}) = \mathrm{Im}\left[\frac{-1}{\varepsilon(\hbar\omega,\overrightarrow{0})}\right]$$

This function exhibits a main peak and several discontinuities. The main peak is located at the silicon plasmon energy E_P = 16.7 eV and is attributed to a prominent collective excitation of valence electrons. The discontinuities correspond to shell effects and can be related to ionization energies of the target material electrons.

The experimental OELF is then modeled using an extended-Drude expression [22] similar to the one used by Akkerman et al. [12–15].

$$\mathrm{OELF} = \sum_j D_j(\hbar\omega) \tag{1}$$

Each element of the sum is used to fit one peak of the experimental curve. The function is thus calculated with six peaks whose position is related to energies with physical meaning: the plasmon energy E_p and ionization energies related to the silicon electron configuration $1s^2\ 2s^2\ 2p^6\ 3s^2\ 3p^2$: one peak for the K-shell (1s), two for the L-shell (2s and 2p) and two for the M-shell (3s and 3p – making it three with the plasmon peak). The details and validation of this fit are presented in [16,17].

The ELF at $\vec{q}\neq\vec{0}$ is then obtained by introducing a quadratic dispersion relation for the expression of one parameter of the function D_j (see [16,17] for more details).

From the ELF, the Differential Cross-Section (DCS) is calculated for each shell for incident particles of kinetic energy E using equation (2):

$$\frac{d\sigma}{d(\hbar\omega)}(E,\hbar\omega) = \frac{1}{\pi \mathrm{N} a_0 E}\int_{q-}^{q+} \mathrm{ELF}(\hbar\omega,\vec{q})\frac{dq}{q} \tag{2}$$

where N is the atomic density of silicon, a_0 the Bohr radius and $q_\pm$ is expressed as: $q_\pm = \frac{\sqrt{2m_e}}{\hbar}(\sqrt{E}\pm\sqrt{E-\hbar\omega})$ for incident electrons, $q_- = \frac{\omega}{v}$ and $q_+ \to \sqrt{2m_e e E_{\max}}/\hbar$ for other incident particles. m_e and e are, respectively, the electron mass and charge, v is the incident particle velocity and E_{max} is the maximal energy transferred to secondary electrons, defined as:

$$E_{\max} = 2m_e c^2\varepsilon(\varepsilon+2) \tag{3}$$

with $\varepsilon = E/Mc^2$ for an incident particle of kinetic energy E and mass M.

One DCS is calculated for each of the six peaks used to fit the experimental OELF: in Eq. (2), instead of using the complete expression of the ELF, it is decomposed according to Eq. (1) and one DCS is calculated for each element of the sum, i.e. each of the six peaks of the ELF. To get the DCS for a given shell, the contribution of, respectively, three, two and one peaks are then summed for, respectively, the M-, L- and K-shell. A second integration over the energy transfer $\hbar\omega$ gives the cross-section as a function of the incident particle energy E.

3. Validation and range of applicability of inelastic cross-sections

3.1. Incident protons

For protons, the resulting partial cross-sections, so called "MuElec" cross sections, calculated for each shell are reported in Fig. 1, as a function of the incident particle energy (for the L- and M-shells, two and three peaks of the ELF are summed, respectively). They are compared with results from calculations using the semi-classical Gryzinski's model [23]. For the M-shell, the agreement is good above 50 keV, with less than 20% difference between both cross-sections. This is particularly important since the M-shell is the main contributor in the energy-loss process. Below this energy, large differences occur; this was already observed for incident electrons below 50 eV in [17]. Indeed, the dielectric function theory is a first Born approximation theory, which is known to fail at low incident energy. Higher-order corrections need to be added, that may be considered in future work, i.e. the Barkas-Andersen and Bloch corrections [24]. While these corrections are usually directly applied to the stopping power calculations, adding respectively a Z_{eff}^3- and Z_{eff}^4-correction term to the classical Z_{eff}^2-proportional stopping power formulation, they can be adapted to be used in the differential cross section formulation, as done in [25].

For now, considering the very large differences between this work's cross sections and Gryzinski's calculations below 50 keV, this value will be taken as the lowest limit of validity for this model for incident protons.

For, the L-shell, the measurements performed by Ariyasinghe et al. are also reported [26]. The agreement between all data is reasonable between 50 and 150 keV (less than an order of magnitude

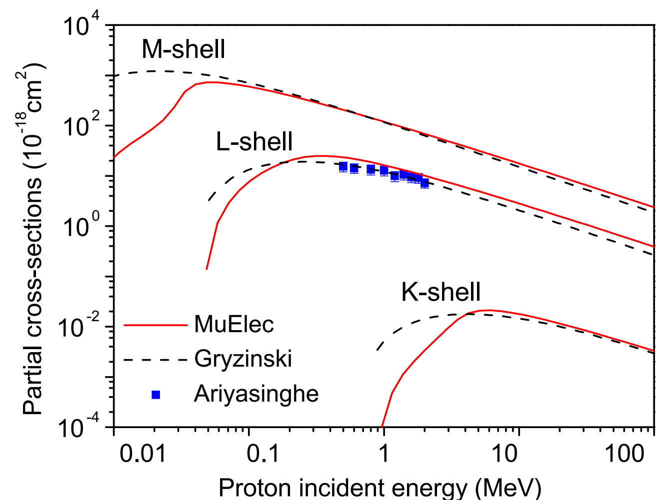

Fig. 1. Calculated proton partial cross-sections compared to the calculations from Gryzinski's classical model [23] and experimental results of Ariyasinghe for the L-shell [26].

of difference and even less than 50% above 80 eV) and good (less than 20% difference) above this energy.

Finally, the K-shell cross-section is in good agreement with Gryzinski's calculations from 5 MeV (less than 20% difference). The difference is large below this energy, but this is not crucial, since the cross-section is three orders of magnitude lower than the L and M-shell; the contribution to the energy-loss process is thus limited.

The proton stopping power is then calculated using the following equation:

$$S(E) = N \int_0^{E/2} \hbar\omega \frac{d\sigma}{d(\hbar\omega)} d(\hbar\omega)$$

It is shown in Fig. 2, along with Konac et al.'s fit on experimental data [27] and data from the PSTAR database [28]. The results from this work's calculation are close to the published data in the 50 keV–100 MeV range, with less than 10% difference.

The maximum energy transferred to secondary electrons by incident protons or heavy ions is limited by the upper limit of validity of the ionization model for incident electrons (50 keV) presented in [16,17]. The maximal energy of incident protons and ions is thus limited to 23 MeV/nucleon – when only the MuElec models are used. Above 23 MeV/nucleon, the simulation may generate high-energy electrons, but their transport is not properly treated by the MuElec inelastic model for electrons. Relativistic corrections should be taken into account to increase this upper limit of validity, as done by Francis et al. [29] for the Geant4-DNA extension, using a formulation proposed by Bousis et al. in [30].

3.2. Incident heavy ions

For incident ions with mass M and charge Z, the inelastic cross-section σ_M is directly related to the proton inelastic cross-section σ_{m_P} through Eq. (4):

$$\sigma_M(E) = Z_{eff}^2 \sigma_{m_P}\left(\frac{m_P}{M}E\right) \quad (4)$$

where m_P and M are, respectively, the proton and ion mass. The effective charge Z_{eff} is calculated according to Barkas formula [31]:

$$Z_{eff} = Z\left[1 - \exp(-125\beta Z^{-2/3})\right] \quad (5)$$

with Z the ion charge, $\beta = v/c$ and v the incident ion velocity.

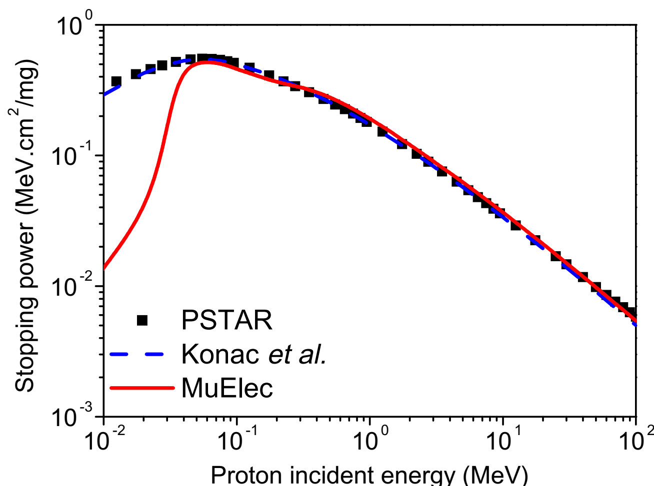

Fig. 2. Calculated proton stopping power (red solid line) compared to the Konac et al.'s fit on experimental data [27] and to the data from the PSTAR database [28]. (For interpretation of the references to colour in this figure legend, the reader is referred to the web version of this article.)

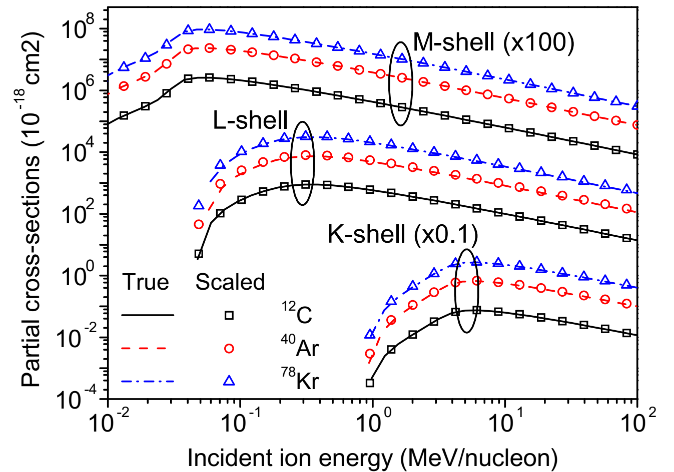

Fig. 3. Partial cross-sections for three different ions calculated either by integration of Eq. (2) ("true" cross-section) or using the scaling formula (4) ("scaled" cross-sections).

To check the validity of the scaling formula (4), the cross-sections are calculated for three different ions (carbon, argon and krypton), either using the complete calculation corresponding to the integration of Eq. (2) or using the scaling formula calculating ion cross-sections from proton one. The results are reported in Fig. 3 as partial cross-sections as a function of the incident ion energy per nucleon. In Fig. 3, the M-shell and K-shell cross-sections are multiplied, respectively, by factors of 100 and 0.1 to ease the differentiation between shells. Both calculation methods give very similar results for all shells and all ions, thus comforting the appropriateness of the scaling formula.

4. Implementation of the MuElec models in Geant4

The goal of this work is to implement the needed parameters and classes for low energy electron generation by incident proton and heavy ions in silicon in the Monte Carlo simulation tool Geant4, using the existing frame of the Geant4-DNA package as a basis. The software design is the same as for the Geant4-DNA package described in [10]. All these developments are included in the Geant4 low energy electromagnetic physics category of the Geant4 toolkit.

The new classes implemented for silicon are derived from Geant4-DNA classes, with only minor modifications. According to the software design described in [10], a physical interaction is described by a "physics process" that can evoke several "models". The process considered here for incident protons and heavy ions is inelastic interactions. It is described by a dedicated Geant4 "process class", namely G4MuElecInelastic. Here, there is only one model for this process, also described by a dedicated Geant4 class: G4MuElecInelasticModel. These process and model classes actually treat both incident electrons and hadrons. They are responsible for the computation of the physical interaction total cross section, as well as for the generation of the final state products, such as the production of secondary particles, according to the corresponding model. The model class needs tabulated differential and total cross-sections as input parameters; they are stored in the database of the Geant4 toolkit in text form, tabulated for protons over the previously determined range of application, i.e. 0.05–23 MeV/nucleon. For incident heavy ions, the cross sections are recalculated at the initialization stage of the simulation, following the scaling formula (4).

To calculate the ejection angle of the produced electron θ, we use energy and momentum conservation, following the two-body

kinematics; the polar angle is then given as follows, with respect to the incident particle movement direction:

$$\cos^2\theta = \frac{\Delta E}{E_{\max}}$$

with $\Delta E = \hbar\omega - E_b$ and E_{max} as defined in Eq. (3). E_b is the binding energy of the shell from which the secondary electron is emitted.

Contrary to incident electrons, no specific "MuElec" elastic process is defined for protons and heavy ions. Elastic scattering can be handled by the multiple scattering model of Urban especially adapted for the standard Geant4 processes ("G4hMultipleScattering" class) [32]. Since the standard processes, including multiple scattering, are recommended for energies above 1 keV in Geant4, this model fully applies to the particles covered by the energy range of application of MuElec models (50 keV–23 MeV).

It is worth highlighting here that, while in the other Geant4 ionization models (Standard and Low energy) the energy loss process is divided in two regions – continuous and discrete energy loss – by a secondary production threshold energy (respectively >1 keV and >250 eV), MuElec follows a discrete approach for particle transport on its entire range of applicability. In other words, MuElec processes simulate explicitly all interactions on a step-by-step basis, to reconstruct precisely track structures of ionizing particles at nanometer scale. While the goal of such simulations is really focused on the result accuracy, high computing performance is required and simulation time can quickly become prohibitive. The on-going effort in the Geant4 collaboration for the development of a multi-threading version of Geant4 (Geant4-MT – a first prototype version is already available [33]) could thus be very interesting to overcome this limitation. For now, only the most common physics-lists have been adapted for and tested to be used within this framework; it would be very useful to eventually adapt MuElec processes and models as well, to reduce simulation times.

5. Simulation of proton tracks in silicon

Fig. 4(a) presents a 3D visualization of 20 protons with an incident energy of 10 MeV passing through a 2 × 2 × 2 μm^3 silicon volume, extracted from Geant4 using our models. Fig. 4(b) presents a similar visualization extracted from a simulation using the Geant4 existing physics list G4EmLivermorePhysics, with Livermore low energy models for secondary electrons. In both cases, the proton follows a straight line (in blue) and emits electrons (in red) of comparable ranges. The increased number of secondary electrons generated with our models is obvious, as highlighted in the zooms. To further test the model, various quantities are extracted from the simulations and compared with results obtained with other calculation codes.

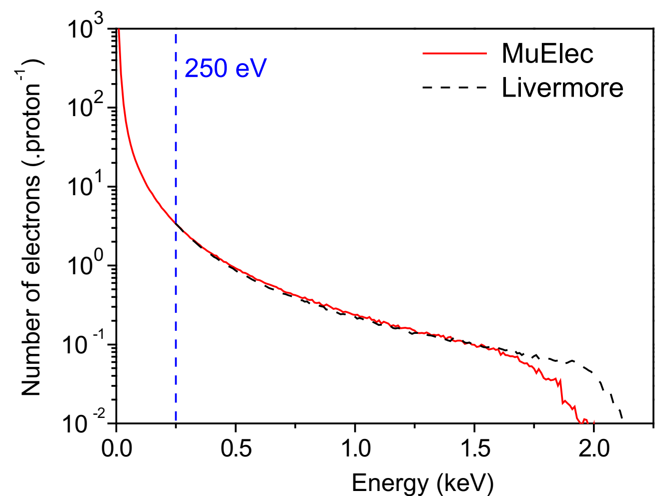

Fig. 5. Number of secondary electrons generated by 1 MeV protons as a function of their energy, for simulations performed using the G4EmLivermorePhysics physics list and MuElec models.

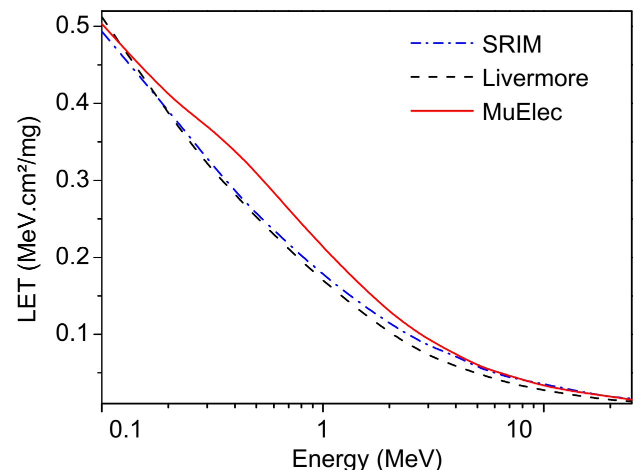

Fig. 6. LET value in silicon depending on the incident proton energy, averaged in a 100 nm-thick silicon layer, as calculated with SRIM and simulated in Geant4, using either the G4EmLivermorePhysics physics list or the MuElec models for electron and proton ionization.

5.1. Energy spectrum

The energy spectrum of secondary electrons is first checked. The results extracted from simulations are reported in Fig. 5, for

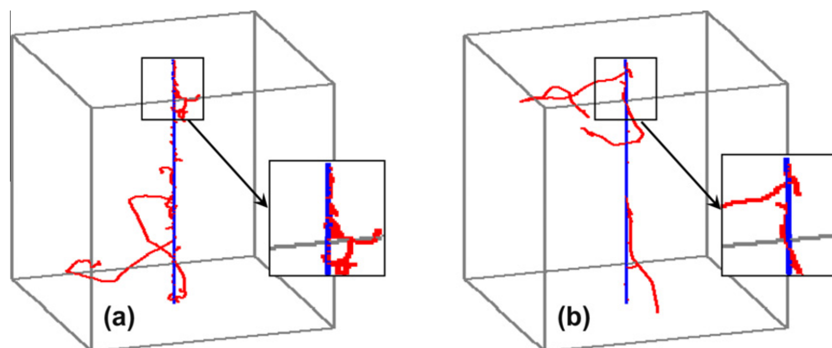

Fig. 4. Geant4 simulation of 20 protons of initial energy 10 MeV passing through a 2 µm silicon cube obtained using (a) our MuElec models and (b) the G4EmLivermorePhysics physics list. The electrons appear as red lines, the proton as a blue line. (For interpretation of the references to colour in this figure legend, the reader is referred to the web version of this article.)

1 MeV protons incident in a 2 µm silicon cube as obtained from simulations performed with the MuElec models and G4EmLivermorePhysics physics list. Above 250 eV, both models give close numbers of generated electrons. Below 250 eV, the G4EmLivermorePhysics physics list does not generate electrons anymore, while our model fully takes into account these low-energy electrons. This confirms the observations made regarding Fig. 4.

The difference between the two models for the production of the highest energy electrons are due to the tabulation of the differential cross sections implemented in Geant4 for MuElec. Increasing the number of points in the table decreases the gap between the two curves for high energy electrons; however, the calculation time is then slower. Therefore, a trade-off has to be found. Given the probability of occurrence for these high energy electrons, it does not dramatically impact the simulation results. This is confirmed by the results seen in the following.

5.2. Linear energy transfer (LET)

The LET (Linear Energy Transfer) is then extracted from simulation. This is mainly to check the correct implementation of the model in Geant4, the LET being equivalent to the stopping power previously calculated. The deposited energy, averaged over a 100 nm thick silicon film for 1000 incident protons, is extracted from Geant4 simulations, using either the G4EmLivermorePhysics physics list or the MuElec models for electron and proton ionization. The results are reported in Fig. 6, as a function of the incident proton energy. The LET as calculated from SRIM/TRIM simulation [34] over the same silicon thickness is also reported, SRIM being the commonly used reference software for such calculation.

While the general trend and the order of magnitude are consistent between all three models, MuElec seems to overestimate the LET for incident protons for energies between 0.2 keV and 2 MeV, with a maximum overestimation of 20% at 0.5 MeV, as compared to SRIM. This is directly related with the overestimation in the L-shell cross-section represented in Fig. 1. Akkerman et al. encountered the same issue in [13]. The problem could come from uncertainties in the experimental OELF which are propagated when fitting it with a sum of extended-Drude functions. Work is in progress to improve this L-shell cross-section calculation.

5.3. Projected range

To verify that the combination of the G4hMultipleScattering class and MuElec models in a Geant4 application is indeed feasible, projected ranges are then extracted from Geant4 simulations. Results are reported in Fig. 7 and compared with the results obtained with G4EmLivermorePhysics. Since there is no MuElec model for protons below 50 keV, the particles are killed below this energy and the corresponding range R obtained with G4EmLivermorePhysics is added to the MuElec range, so that in the figure, for an incident energy E:$R_{MuElec}(E) = R_{MuElec}(E$ down to 50 keV$) + R_{G4EmLivermorePhysics}(50$ keV$)$.

Data from the PSTAR database [28] are also reported in the figure as reference.

Between 50 keV and 0.5 MeV, MuElec projected ranges are overestimated compared to data from the PSTAR database, following the same trend as results obtained with the G4EmLivermorePhysics physics list. Above 0.5 MeV, MuElec ranges are systematically underestimated, by ~20%. This is consistent with the LET overestimation in Fig. 6.

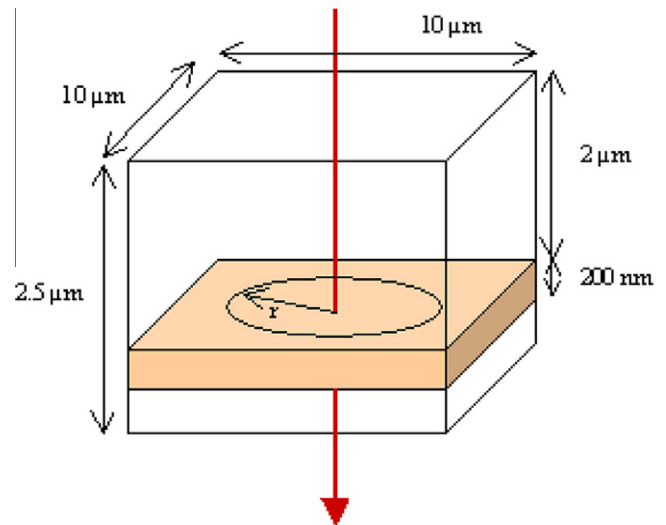

Fig. 8. Geometry used to simulate radial dose distributions.

5.4. Radial ionization profiles

The radial deposited energy is finally simulated. The geometry is shown in Fig. 8. The deposited energy is recorded in the colored area only; this 200 nm silicon layer is chosen to be representative

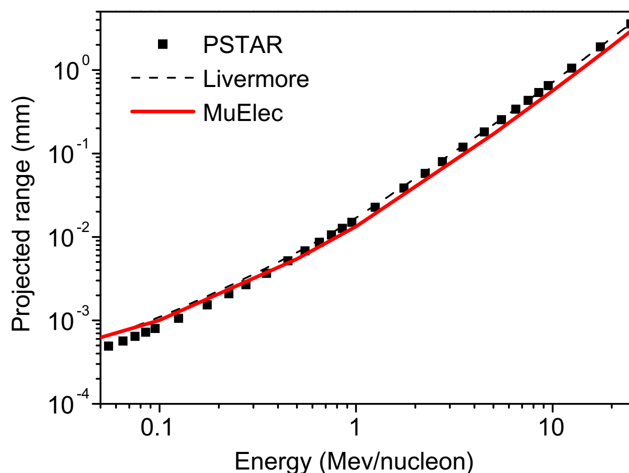

Fig. 7. Projected range in silicon depending on the incident proton energy: data from the PSTAR database [28] and results from Geant4 simulation, using either the G4EmLivermorePhysics physics list or the MuElec models.

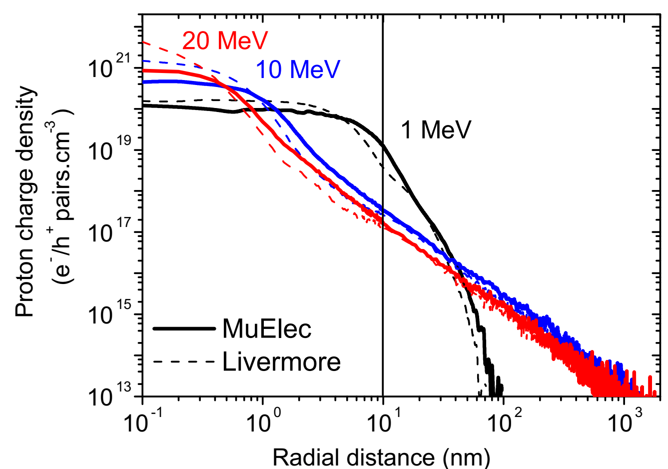

Fig. 9. Average charge density generated by 1, 10 and 20 MeV protons extracted from Geant4 simulations using either the G4EmLivermorePhysics physics list (dotted lines) or the MuElec models (solid lines).

of the active silicon layer in a standard SOI (silicon on insulator) technology [35–37]. It is also sufficiently thick to get good statistics with a reasonable number of incident particles and thin enough for the LET to be considered constant along the track.

To calculate the radial track structure, the deposited energy is recorded as a function of the radial distance to the ion path, and converted to a density of electron/hole pairs, as done in [6], with 3.6 eV the average energy needed to create an electron/hole pair in silicon [38]. The resulting average proton charge density calculated using the MuElec models and G4EmLivermorePhysics physics list are plotted in Fig. 9 for 1, 10 and 20 MeV incident protons. In these simulations, the elastic scattering of protons is voluntarily turned off, to represent the average effect of a single incident particle. The track is averaged over 10^4 incident particles for the G4EmLivermorePhysics physics list. For MuElec, given the much longer simulation time ($\sim 1000\times$ longer), only 10^3 incident particles are used. Since the secondary electrons are much more numerous, this is sufficient to get a good description of the proton track.

As expected, the main differences between both models appear at low radius: along the ion path, the density calculated with the MuElec model is lower than the one calculated with the G4EmLivermorePhysics physics list; then it decreases more slowly. This can be attributed to the transport of low-energy electrons (below 250 eV): in the G4EmLivermorePhysics physics list, these electrons are not generated and their energy is deposited locally, leading to an artificially high density along the ion path; in the MuElec model, the energy is radially distributed throughout the first 10 nm.

6. Conclusion

New process and model classes, called "MuElec", are implemented in the open-access particle-matter interaction simulation toolkit Geant4 for the simulation of proton and heavy ion tracks in silicon. They take into account the production of low energy electrons down to 16.7 eV. Another part of the MuElec extension previously presented [16,17] deals with the transport of these low energy electrons. The theory is similar to the one proposed by Akkerman et al. and is implemented following a similar scheme as the Geant4-DNA extension. A comparison with data from the literature allow to validate the MuElec cross sections for incident protons in the energy range 50 keV–23 MeV. The models are then implemented in Geant4 and used to simulate proton tracks. Various physical quantities (spectra, LET, projected range, radial dose) are extracted from these simulations and compared with data from the literature and with results obtained with other Geant4 models. Some limitations of the code are identified; in particular the L-shell cross section seems to be overestimated. All these results are based solely on the dielectric function theory and various corrections to this first Born approximation theory may be implemented to widen the range of applicability of the code and solve the remaining issues. They will be presented in a dedicated publication.

Despite the identified limitations, the generation of low-energy electrons is shown to result in more physically meaningful low-energy secondary electron tracks, which significantly modifies the proton and ion track core. These results form a solid basis for a better understanding of electron, proton and heavy ion track simulations, that should be very useful for the future study of advanced electronic components under irradiation [39]. The MuElec extension will be made publicly available in the Geant4v9.6 beta release in June 2012.

Acknowledgements

The author thank A. Akkerman for his very useful hints about the model. We also thank A. Mantero, V. Ivantchenko, Z. Francis and S. Incerti for the help they provided in developing the code.

References

[1] The 2006 International Technology Roadmap for Semiconductor ITRS (Online). Available at: <http://www.itsr.net/Links/2006update/2006UpdateFinal>.
[2] S. Agostinelli, J. Allison, K. Amako, J. Apostolakis, H. Araujo, P. Arce, M. Asai, D. Axen, S. Banerjee, G. Barrand, et al., Nucl. Instr. Meth. A 506 (2003) 250.
[3] J. Allison, K. Amako, J. Apostolakis, H. Araujo, P. Arce Dubois, M. Asai, G. Barrand, R. Capra, S. Chauvie, R. Chytracek, et al., IEEE Trans. Nucl. Sci. 53 (2006) 270.
[4] A.S. Kobayashi, A.L. Sternberg, L.W. Massengill, R.D. Schrimpf, R.A. Weller, IEEE Trans. Nucl. Sci. 51 (2004) 3312.
[5] M.P. King, R.A. Reed, R.A. Weller, M.H. Mendenhall, R.D. Schrimpf, M.L. Alles, E.C. Auden, S.E. Armstrong, M. Asai, IEEE Trans. Nucl. Sci. 57 (2010) 3169.
[6] M. Raine, M. Gaillardin, J.-E. Sauvestre, O. Flament, A. Bournel, V. Aubry-Fortuna, IEEE Trans. Nucl. Sci. 57 (2010) 1892.
[7] M. Raine, G. Hubert, M. Gaillardin, L. Artola, P. Paillet, S. Girard, J.-E. Sauvestre, A. Bournel, IEEE Trans. Nucl. Sci. 58 (2011) 840.
[8] R.A. Weller, M.H. Mendenhall, R.A. Reed, R.D. Schrimpf, K.M. Warren, B.D. Sierawski, L.W. Massengill, IEEE Trans. Nucl. Sci. 57 (2010) 1726.
[9] G.A.P. Cirrone, G. Cuttone, F. Di Rosa, L. Pandola, F. Romano, Q. Zhang, Nucl. Instr. Meth. A 618 (2010) 315.
[10] S. Incerti, A. Ivanchenko, M. Karamitros, A. Mantero, P. Moretto, H.N. Tran, B. Mascialino, C. Champion, V.N. Ivanchenko, M.A. Bernal, et al., Med. Phys. 37 (2010) 4692.
[11] S. Incerti, G. Baldacchino, M. Bernal, R. Capra, C. Champion, Z. Francis, P. Gueye, A. Mantero, B. Mascialino, P. Moretto, et al., International Journal of Modeling, Simulation, and Scientific Computing 1 (2010) 157.
[12] A. Akkerman, J. Barak, IEEE Trans. Nucl. Sci. 49 (2002) 3022.
[13] A. Akkerman, J. Barak, D. Emfietzoglou, Nucl. Instr. Meth. B 227 (2005) 319.
[14] A. Akkerman, M. Murat, J. Barak, J. Appl. Phys. 106 (2009) 113703.
[15] D. Emfietzoglou, A. Akkerman, J. Barak, IEEE Trans. Nucl. Sci. 51 (2004) 2872.
[16] A. Valentin, M. Raine, J.-E. Sauvestre, Nuclear Science Symposium and Medical Imaging Conference, 2010.
[17] A. Valentin, M. Raine, J.-E. Sauvestre, M. Gaillardin, P. Paillet, Nucl. Instr. Meth. B (2012), submitted for publication.
[18] D. Emfietzoglou, K. Karava, G. Papamichael, M. Moscovitch, Phys. Med. Biol. 48 (2003) 2355.
[19] D. Emfietzoglou, M. Moscovitch, Nucl. Instr. Meth. B 193 (2002) 71.
[20] D. Edwards, Handbook of Optical Constants, Academic Press, New York, 1985.
[21] F. Biggs, R. Lighthill, Report SAND87-0070, 1988.
[22] R.H. Ritchie, A. Howie, Philos. Mag. 36 (1977) 463.
[23] M. Gryzinski, Phys. Rev. 138 (1965) 336.
[24] J.C. Ashley, J. Phys.: Condens. Matter 3 (1991) 2741.
[25] Z. Tan, Y. Xia, Nucl. Instr. Meth. B 269 (2011) 328.
[26] W.M. Ariyasinghe, H.T. Awuku, D. Powers, Phys. Rev. A 42 (1990) 3819.
[27] G. Konac, C. Klatt, S. Kalbitzer, Nucl. Instr. Meth. B 146 (1998) 106.
[28] M.J. Berger, J.S. Coursey, M.A. Zucker, J. Chang, NIST Reports (2005).
[29] Z. Francis, S. Incerti, R. Capra, B. Mascialino, G. Montarou, V. Stepan, C. Villagrasa, Appl. Radiat. Isot. 69 (2011) 220.
[30] C. Bousis, D. Emfietzoglou, P. Hadjidoukas, H. Nikjoo, A. Pathak, Nucl. Instr. Meth. B 266 (2008) 1185.
[31] W.H. Barkas, Nuclear Research Emulsions, vol. 1, Academic Press Inc., New York, 1963, p. 371.
[32] Geant4 Physics Reference Manual (Online). Available at: <http://geant4.web.cern.ch/UserDocumentation/UsersGuides/PhysicsReferenceManual/fo/PhysicsReferenceManual.pdf>.
[33] Geant4-MT Prototype (Online). Available at: <http://geant4.cern.ch/support/download_MT_proto.shtml>.
[34] SRIM (Online). Available at: <http://www.srim.org>.
[35] J.-P. Colinge, Silicon-On-Insulator Technology: Materials to VLSI, Kluwer Academic Publishers, 1991, p. 48.
[36] O. Musseau, IEEE Trans. Nucl. Sci. 43 (1996) 603.
[37] SOITEC (Online). Available at: <http://www.soitec.com>.
[38] C.A. Klein, J. Appl. Phys. 39 (1968) 2029.
[39] M. Raine, A. Valentin, M. Gaillardin, P. Paillet, NSREC 2012, accepted for oral presentation.